NASA TECHNICAL MEMORANDUM

NASA TM X-73433

NASA TM X-73433

PERFORMANCE OF A RECOVERABLE TUG FOR PLANETARY MISSIONS INCLUDING USE OF PERIGEE PROPULSION AND CORRECTIONS FOR NODAL REGRESSION

by Janos Borsody
Lewis Research Center
Cleveland, Ohio 44135

TECHNICAL PAPER to be presented at
Astrodynamics Conference cosponsored by the
American Institute of Aeronautics and Astronautics
and the American Astronomical Society
San Diego, California, August 18-20, 1976

PERFORMANCE OF A RECOVERABLE TUG FOR PLANETARY MISSIONS INCLUDING USE OF PERIGEE PROPULSION AND CORRECTIONS FOR NODAL REGRESSION

Janos Borsody
Lewis Research Center
National Aeronautics and Space Administration
Cleveland, Ohio

Abstract

Mathematical equations are derived by using the Maximum Principle to obtain the maximum payload capability of a reusable Tug for planetary missions. The mathematical formulation includes correction for nodal precession of the Space Shuttle orbit. The Tug performs this nodal correction in returning to this precessed orbit. The sample case analyzed represents an inner planet mission as defined by the declination (fixed) and right ascension of the outgoing asymptote and the mission energy. Payload capability is derived for a typical cryogenic Tug and the sample case with and without perigee propulsion. Optimal trajectory profiles and some important orbital elements are also discussed.

E-5782

Introduction

At the present time NASA is developing a reusable Space Shuttle (SS) that will carry payloads to low Earth orbit. For missions beyond low Earth orbit the SS will carry in its cargo bay (in addition to the payload) a propulsive stage that will be deployed in low Earth orbit and will deliver the payload to its required injection conditions.

This propulsive stage may be expended after payload delivery, or it may be returned to a waiting SS for a flight back to Earth. Expendable stage performance can be analyzed with techniques developed for expendable launch vehicles and will not be discussed herein.

In this paper, the maximum performance capability of a reusable stage (Tug) is derived for planetary missions. This is a complex mathematical optimization problem since the Tug is beyond Earth-escape energy at payload injection and must perform a retroburn to return to an Earth orbit. Since this retroburn occurs far from Earth, large velocity losses are encountered, as will be discussed.

The mathematical optimization problem is formulated by using the Maximum Principle. State and associated adjoint equations are numerically integrated to determine the instantaneous position and velocity of the Tug. To obtain the maximum payload capability, variational final conditions are derived by using the Maximum Principle, and the two-point boundary value problem is solved by using a Newton-Raphson iteration technique. The required partial derivatives of final conditions with respect to initial conditions are evaluated by perturbing the initial conditions one at a time, integrating the state and adjoint equations, and observing the changes in final conditions.

Reusable Tug trajectories, including nodal correction without perigee propulsion, have been investigated in reference 1. The analysis presented herein extends the results of this reference by optimizing the Tug total trip time and introducing perigee propulsion. Total trip time is defined as the elapsed time from the start of the first outbound burn to return to the SS orbit for rendezvous. For perigee propulsion the continuous outbound burn required to reach payload injection conditions is split into two burns separated by an optimum coast time. The present analysis also includes nodal regression of the SS orbit. Nodal regression is caused by the Earth's oblateness, which induces a rotation of the SS orbital plane of about 0.3 deg/hr about the polar axis. Since the Tug must return to the SS orbit and the SS does not have performance capability to substantially alter its line of nodes, the Tug is assumed to make all necessary nodal corrections for rendezvous.

As a sample case, payload capability is derived as a function of the declination of the outgoing asymptote with and without perigee propulsion for a typical cryogenic Tug configuration and an inner planet mission. A discussion of optimal trajectory profiles and SS launch time constraints is included.

Analysis

Trajectory Profiles and Assumptions

A trajectory profile for the perigee propulsion case is illustrated in sketch (a). Tug and payload are deployed in a low Earth orbit by the Space Shuttle (SS). The first outbound burn is initiated at an optimal point along this orbit. The length of the burn is determined during the optimization process in solving the two-point boundary value problem. At the end of this burn an elliptic orbit is established with a relatively long period. Tug and payload then coast along this orbit to a point just before perigee, where a second outbound burn is performed that accelerates the payload to the given injection conditions. The time at which the second outbound burn starts is also determined during the optimization. Planetary injection conditions are defined by

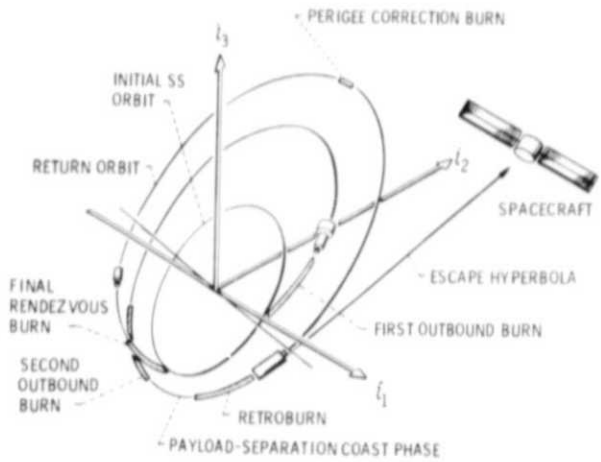

(a)

specifying the mission energy and the declination of the outgoing asymptote. The right ascension of the outgoing asymptote is not included as a final condition, because any right ascension may be obtained by selecting the proper SS launch time. This is discussed in more detail later. After the Tug reaches the given injection conditions, the Tug thrust is terminated and a fixed coast phase is initiated. During this coast the Tug and the payload are separated, and the Tug is turned around to orient it for the retroburn that follows. During this retroburn the energy is reduced below Earth-escape energy, and the Tug enters an intermediate elliptic return orbit. Retroburn terminates when a given total trip time is satisfied. Total trip time is defined as the elapsed time from the start of the first outbound burn to return to the SS orbit for rendezvous. The retroburn is followed by a coast phase to the apogee of the intermediate orbit, where a small perigee correction burn is executed. This is followed by a coast phase to perigee and a final rendezvous burn.

The flight profile for the case without perigee propulsion is the same as just discussed with the exception that the first outbound burn continues until the given injection conditions are satisfied and thus the coast in elliptic orbit and the second outbound burn are eliminated.

To obtain solutions to the two-point boundary value problem and to simplify the analysis, a number of assumptions were made. These assumptions are discussed in the following paragraphs:

(1) The perigee correction and final circularization burns were assumed to be ideal impulsive. This assumption was made to reduce the sensitivity and consequently improve the convergence characteristics of the two-point boundary value problem. If the corresponding state equations are stable, the adjoint equations will have unstable roots. Since total trip time for the problem under consideration is of the order of 1 day (based on the results of ref. 1), errors introduced in the numerical integration of state and adjoint equations will be greatly amplified. These errors will affect the finite difference partial derivatives and consequently the convergence of the Newton-Raphson iteration. With this assumption, the problem is numerically integrated only to the end of the retroburn, and the remaining portion of the trajectory is calculated in closed form (impulsively).

(2) A circular SS orbit is assumed. This assumption is made to eliminate the constraint on the line of apsides. For elliptic SS orbits the Tug's orbit at the end of final rendezvous burn, besides being in the same orbital plane, must have its line of apsides coincident with that of the SS orbit. Using a circular SS orbit removes this constraint, and rendezvous is accomplished by small changes in total trip time. The trip time has to be adjusted so that the Tug and SS will be at the same point along the orbit at final rendezvous burn completion.

(3) A spherical nonrotating Earth model is used. This assumption is made to simplify the equations of motion and the adjoint equations. A nonspherical Earth model could be included with relatively little change in the analysis. As a result of this assumption the nodal precession of the intermediate Tug orbits becomes zero, and the Tug corrects for SS orbit nodal precession only. This gives somewhat conservative Tug performance since, if the Tug orbits were allowed to precess, the total nodal correction required of the Tug would be slightly reduced, and consequently payload capability would increase. Nodal precession of the Tug orbits for the nominal mission is less than 0.2 deg without perigee propulsion and less than 0.4 deg with perigee propulsion, as compared with an SS orbit nodal precession of approximately 8 deg.

(4) The SS orbit nodal precession is computed from the following equation:

$$\Delta\Omega = -\frac{J\sqrt{G}}{R_E^{3/2}} T_D \left(\frac{R_E}{p}\right)^{7/2} \left(1 - e^2\right)^{3/2} \cos i \qquad (1)$$

This equation was derived in reference 2. Nodal precession depends on the SS orbital parameters and the total trip time T_D.

Basic Equations Governing the Problem

Variables and other notation used in the following discussion are defined in the appendix. Equations describing the flight of a rocket in an inverse-square gravitational field are

$$\dot{\bar{V}} = -\frac{G}{r^3}\bar{r} + \frac{V_e\beta(\xi)}{m}\hat{f} \tag{2}$$

$$\dot{\bar{r}} = \bar{V} \tag{3}$$

$$\dot{m} = -\beta(\xi) \tag{4}$$

$$\dot{\xi} = 1 \tag{5}$$

$$\hat{f}\cdot\hat{f} - 1 = 0 \tag{6}$$

In these equations, r, V, and m represent instantaneous radius, velocity, and mass, respectively; V_e is the engine exhaust velocity; β is the mass flow rate; and $\hat{f}$ is the unit thrust direction, which must be determined. The state variable ξ was introduced to remove the explicit time dependence of mass flow rate from the equations of motion so that the Maximum Principle could be applied to this problem. The superscripts $-$ and $\hat{}$ represent vector and unit vector quantities, and $\cdot$ is the total derivative of the particular variable with respect to time.

By using the Hamiltonian formulation of the variational calculus, the costate equations may be obtained from the so-called Hamiltonian on each subarc. The Hamiltonian is

$$H = \bar{\lambda}\cdot\dot{\bar{V}} + \bar{\mu}\cdot\dot{\bar{r}} + \sigma\dot{m} + \tau\dot{\xi} + \gamma(\hat{f}\cdot\hat{f} - 1) \tag{7}$$

In this equation, $\bar{\lambda}$, $\bar{\mu}$, σ, and τ are the adjoint variables associated with the problem. The constraint associated with the thrust direction is also adjoined to H by γ. From equation (7) the time derivatives of the adjoint variables are given by

$$\dot{\bar{\lambda}} = -\bar{\mu} \tag{8}$$

$$\dot{\bar{\mu}} = \frac{G}{r^3}\left[\bar{\lambda} - 3(\bar{\lambda}\cdot\hat{r})\hat{r}\right] \tag{9}$$

$$\dot{\sigma} = \frac{V_e\beta}{m^2}(\bar{\lambda}\cdot\hat{f}) \tag{10}$$

$$\dot{\tau} = -K\frac{\partial\beta}{\partial\xi} \tag{11}$$

where

$$K = \frac{V_e}{m}(\bar{\lambda}\cdot\hat{f}) - \sigma \tag{12}$$

The thrust direction that minimizes the Hamiltonian is given by

$$\hat{f} = \hat{\lambda} \tag{13}$$

and

$$\gamma = -\frac{V_e\beta}{2m}\lambda \tag{14}$$

State equations (2) to (5) and adjoint equations (8) to (11) make up a set of first-order nonlinear differential equations that must be numerically integrated in order to obtain a solution to the two-point boundary value problem. Optimum thrust direction is along the unit vector given by equation (13).

Trajectory Constraints

In this section, constraints on the problem are discussed in more detail. Sketch (b) illustrates a simplified trajectory profile from a given initial orbit to the end of retroburn. Events a_1 and b_1 indicated on the sketch are the times at the beginning and end of phase 1, respectively.

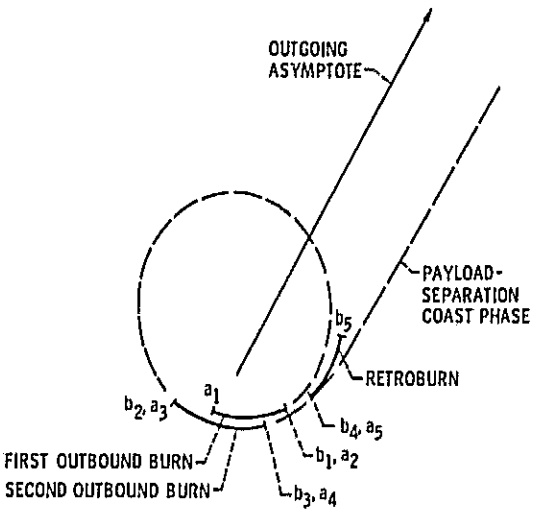

(b)

The first outbound burn is initiated at time a_1 ($a_1 = 0$) at an optimal point in the initial SS circular inclined orbit. Main engine thrust terminates at time b_1, which is selected to give maximum payload. At this time an elliptic orbit is established and the Tug coasts along this orbit to a point near perigee (time b_2). Second outbound burn starts at time a_3 ($a_3 = b_2$) and continues until the specified payload injection conditions are reached at time b_3. Time a_4 ($a_4 = b_3$) is the beginning

of a fixed payload-separation coast that continues until time b_4. Tug retroburn starts at time a_5 ($a_5 = b_4$) and ends at b_5. Retroburn is followed by ideal impulsive apogee and perigee burns and associated coast phases. With this time convention, constraints q_i governing the problem can be written mathematically as follows:

$$q_1 = r(a_1) - r_1 = 0 \tag{15.1}$$

$$q_2 = V(a_1) - V_1 = 0 \tag{15.2}$$

$$q_3 = \bar{r}(a_1) \cdot \bar{V}(a_1) = 0 \tag{15.3}$$

$$q_4 = \hat{h}(a_1) \cdot \hat{\ell}_3 - \cos i_1 = 0 \tag{15.4}$$

$$q_5 = -\hat{h}(a_1) \cdot \hat{\ell}_2 - \cos \Omega_1 \sin i_1 = 0 \tag{15.5}$$

$$q_6 = m(a_1) - m_1 = 0 \tag{15.6}$$

$$q_7 = \xi(a_1) - a_1 = 0 \tag{15.7}$$

$$\bar{q}_8 = \bar{r}(a_2) - \bar{r}(b_1) = \bar{0} \tag{15.8}$$

$$\bar{q}_9 = \bar{V}(a_2) - \bar{V}(b_1) = \bar{0} \tag{15.9}$$

$$q_{10} = m(a_2) - m(b_1) = 0 \tag{15.10}$$

$$q_{11} = \xi(a_2) - \xi(b_1) = 0 \tag{15.11}$$

$$\bar{q}_{12} = \bar{r}(a_3) - \bar{r}(b_2) = \bar{0} \tag{15.12}$$

$$\bar{q}_{13} = \bar{V}(a_3) - \bar{V}(b_2) = \bar{0} \tag{15.13}$$

$$q_{14} = m(a_3) - m(b_2) = 0 \tag{15.14}$$

$$q_{15} = \xi(a_3) - \xi(b_2) = 0 \tag{15.15}$$

$$\bar{q}_{16} = \bar{r}(a_4) - \bar{r}(b_3) = \bar{0} \tag{15.16}$$

$$\bar{q}_{17} = \bar{V}(a_4) - \bar{V}(b_3) = \bar{0} \tag{15.17}$$

$$q_{18} = m(a_4) - m(b_3) = 0 \tag{15.18}$$

$$q_{19} = \xi(a_4) - \xi(b_3) = 0 \tag{15.19}$$

$$q_{20} = E\left[r(b_4), V(b_4)\right] - E_D = 0 \tag{15.20}$$

$$q_{21} = \varphi\left[r(b_4), V(b_4)\right] - \varphi_D = 0 \tag{15.21}$$

$$\bar{q}_{22} = \bar{r}(a_5) - \bar{r}(b_4) = \bar{0} \tag{15.22}$$

$$\bar{q}_{23} = \bar{V}(a_5) - \bar{V}(b_4) = \bar{0} \tag{15.23}$$

$$q_{24} = \xi(a_5) - \xi(b_4) = 0 \tag{15.24}$$

$$q_{25} = \hat{r}(b_5) \cdot \hat{h}_o(T_D) = 0 \tag{15.25}$$

$$q_{26} = \hat{V}(b_5) \cdot \hat{h}_o(T_D) = 0 \tag{15.26}$$

$$q_{27} = m(b_5) - m_{II}^{(1/V_e)(\Delta V_a + \Delta V_p)} = 0 \tag{15.27}$$

$$q_{28} = a_2 - b_1 = 0 \tag{15.28}$$

$$q_{29} = a_3 - b_2 = 0 \tag{15.29}$$

$$q_{30} = a_4 - b_3 = 0 \tag{15.30}$$

$$q_{31} = a_5 - b_4 = 0 \tag{15.31}$$

$$q_{32} = a_4 + \Delta t - b_4 = 0 \tag{15.32}$$

$$q_{33} = \xi(a_4) + \Delta t - \xi(b_4) = 0 \tag{15.33}$$

Equations (15.1) to (15.7) express fixed initial conditions at Tug departure from the initial SS orbit. Equations (15.8) to (15.19) give the continuity of radius, velocity, mass, and the dummy variable ξ at the end of the first and second outbound burns and at the beginning of the second outbound burn. Equations (15.20) and (15.21) express the constraints associated with a planetary mission, namely, at injection the payload must have a given energy and declination of the outgoing asymptote. Equations (15.22), (15.23), and (15.24) give the continuity of position, velocity, and ξ at injection. Satisfying equations (15.25) and (15.26) assures that the Tug is in an orbit that has the same inclination at retroburn completion as the SS will have at rendezvous. In other words the flight is planar following the retroburn. The vector $\hat{h}_o$ in equations (15.25) and (15.26) is the unit angular momentum vector of the precessed SS orbit to which the Tug must return. The vector $\hat{h}_o$ is a function of the total trip time. Equation (15.27) is the constraint on Tug mass required at b_5 to perform the apogee and perigee velocity changes and return the Tug empty to the final SS orbit. Equations (15.28) to (15.31) express the continuity of time between different trajectory phases. Equations (15.32) and (15.33) are the fixed payload-separation coast time constraint and the constraint on ξ, respectively.

With these constraints the augmented Hamiltonian (H^*) to be minimized can be written as follows:

$$H^* = m(a_5) - m(b_4) + \sum_{i=1}^{5} H_i + \sum_{i=1}^{33} \epsilon_i q_i \tag{16}$$

where $m(b_4) - m(a_5)$ represents the payload weight dropped during the coast phase, which is to be maximized; and H_i are Hamiltonians during the two outbound burns, the two coast phases, and the retroburn.

Constraints q_i are adjoined to H^* by using arbitrary multipliers ϵ_i. Auxiliary variational boundary conditions may now be derived from this augmented Hamiltonian.

Auxiliary Variational Boundary Conditions

The following auxiliary variational equations must be satisfied by using the Maximum Principle and the augmented Hamiltonian in equation (16) in order to maximize payload:

$$\bar{\lambda}(a_1) = \epsilon_2\hat{V}(a_1) + \epsilon_3\bar{r}(a_1) + \epsilon_4\nabla_{\bar{V}}q_4 + \epsilon_5\nabla_{\bar{V}}q_5 \quad (17.1)$$

$$\bar{\mu}(a_1) = \epsilon_1\hat{r}(a_1) + \epsilon_3\bar{V}(a_1) + \epsilon_4\nabla_{\bar{r}}q_4 + \epsilon_5\nabla_{\bar{r}}q_5 \quad (17.2)$$

$$\bar{\lambda}(a_2) = \bar{\lambda}(b_1) \quad (17.3)$$

$$\bar{\mu}(a_2) = \bar{\mu}(b_1) \quad (17.4)$$

$$\sigma(a_2) = \sigma(b_1) \quad (17.5)$$

$$\tau(a_2) = \tau(b_1) \quad (17.6)$$

$$\bar{\lambda}(a_3) = \bar{\lambda}(b_2) \quad (17.7)$$

$$\bar{\mu}(a_3) = \bar{\mu}(b_2) \quad (17.8)$$

$$\sigma(a_3) = \sigma(b_2) \quad (17.9)$$

$$\tau(a_3) = \tau(b_2) \quad (17.10)$$

$$\bar{\lambda}(a_4) = \bar{\lambda}(b_3) \quad (17.11)$$

$$\bar{\mu}(a_4) = \bar{\mu}(b_3) \quad (17.12)$$

$$\sigma(a_4) = \sigma(b_3) \quad (17.13)$$

$$\bar{\lambda}(a_5) = \bar{\lambda}(b_4) + \epsilon_{20}\nabla_{\bar{V}}E(b_4) + \epsilon_{21}\nabla_{\bar{V}}\varphi(b_4) \quad (17.14)$$

$$\bar{\mu}(a_5) = \bar{\mu}(b_4) + \epsilon_{20}\nabla_{r}E(b_4) + \epsilon_{21}\nabla_{r}\varphi(b_4) \quad (17.15)$$

$$\sigma(a_5) = 1 \quad (17.16)$$

$$\sigma(b_4) = 1 \quad (17.17)$$

$$\tau(a_4) - \tau(b_3) + \tau(a_5) - \tau(b_4) = 0 \quad (17.18)$$

$$\bar{\lambda}(b_5) + \left[\epsilon_{25}\hat{r}(b_5) + \epsilon_{26}\hat{V}(b_5)\right]\cdot\frac{\partial\hat{h}_o}{\partial T_D}\nabla_{\bar{V}}T + \sigma(b_5)\frac{m(b_5)}{V_e}\nabla_{\bar{V}}\Delta V_T + \frac{\epsilon_{26}}{V(b_5)}\left\{\hat{h}_o - \left[\hat{h}_o\cdot\hat{V}(b_5)\right]\hat{V}(b_5)\right\} = \bar{0} \quad (17.19)$$

$$\bar{\mu}(b_5) + \left[\epsilon_{25}\hat{r}(b_5) + \epsilon_{26}\hat{V}(b_5)\right]\cdot\frac{\partial\hat{h}_o}{\partial T_D}\nabla_{\bar{r}}T + \sigma(b_5)\frac{m(b_5)}{V_e}\nabla_{\bar{r}}\Delta V_T + \frac{\epsilon_{25}}{r(b_5)}\left\{\hat{h}_o - \left[\hat{h}_o\cdot\hat{r}(b_5)\right]\hat{r}(b_5)\right\} = \bar{0} \quad (17.20)$$

$$H(a_2) = H(b_1) \quad (17.21)$$

$$H(a_3) = H(b_2) \quad (17.22)$$

$$H(a_5) + H(a_4) - H(b_3) - H(b_4) = 0 \quad (17.23)$$

$$H(b_5) = \left[\epsilon_{25}\hat{r}(b_5) + \epsilon_{26}\hat{V}(b_5)\right]\cdot\frac{\partial\hat{h}_o}{\partial T_D} \quad (17.24)$$

$$\tau(b_5) = 0 \quad (17.25)$$

Equations (17.1) and (17.2) contain six equations and five arbitrary constants. Therefore, there is a variational condition that the initial multipliers must satisfy to maximize payload. Equations (17.3) to (17.13) give the continuity of adjoint variables at the end of the first and second outbound burns and at the beginning of the second outbound burn. These equations can be satisfied directly by setting the multipliers at the beginning of these phases equal to the corresponding multipliers at the end of the previous phase. Multipliers at the end of the payload-separation coast are discontinuous, as shown by equations (17.14) and (17.15). This discontinuity will be computed later. Multiplier σ is continuous and equal to 1 at the end of the payload-separation coast phase (eqs. (17.16) and (17.17)). Equations (17.19) and (17.20) must be satisfied at retroburn completion. They contain six equations and three unknowns (ϵ_{25}, ϵ_{26}, and $\sigma(b_5)$). The three variational conditions available for optimization will be evaluated later. The Hamiltonian is continuous at the completion of the first outbound burn and the start of the second outbound burn, as given by equations (17.21) and (17.22). Equation (17.23) gives the relation the Hamiltonian must satisfy at the end of the second outbound burn and the start of the retroburn. Gradients of return time T, total delta velocity $\Delta V_T = \Delta V_R + \Delta V_P$, and declination φ were derived in reference 1 and will not be reproduced herein. Equation (17.24) gives the Hamiltonian at retroburn completion. The vector $\hat{h}_o$ is a function of the total trip time, or return time, and the required partial derivatives will be evaluated later. Return time is defined as the time from retroburn completion to return to the SS orbit. Equation (17.25) is the boundary condition on the multiplier associated with the dummy variable ξ.

Variational Final Condition at Departure from Initial SS Orbit

To derive the variational final condition contained in equations (17.1) and (17.2), define the vector

$$\overline{C}(t) = \overline{X}(t) \times \overline{V}(t) + \overline{\mu}(t) \times \overline{r}(t) \tag{18}$$

where $\times$ represents the vector or cross product in this equation. The vector $\overline{C}$ is a constant of motion. This can be shown by taking the time derivative of C and substituting equations (2), (3), (8), and (9) for $\dot{\overline{V}}$, $\dot{\overline{r}}$, and $\dot{\overline{\mu}}$, respectively. The time derivative of $\overline{C}$ turns out to be identically zero; therefore, C is a constant of motion.

The variational condition at departure from the initial orbit may now be computed as follows. Compute the $\overline{C}$ vector at a_1 giving

$$\overline{C}(a_1) = (\epsilon_4 \hat{\ell}_3 - \epsilon_5 \hat{\ell}_2) \times \hat{h}(a_1) \tag{19}$$

From this equation the variational final condition is obtained by taking the scalar product with $\hat{h}(a_1)$, giving

$$\overline{C}(a_1) \cdot \hat{h}(a_1) = 0 \tag{20}$$

Evaluation of Discontinuity in State Variables at End of Payload-Separation Coast Phase

To evaluate the discontinuity in $\overline{X}$ and $\overline{\mu}$ at time a_5, two arbitrary constants (ϵ_{20} and ϵ_{21}) must be evaluated in equations (17.14) and (17.15). These constants are evaluated in this section. Take the vector products of equation (17.14) with $\overline{V}$ and (17.15) with $\overline{r}$, add the resulting vector equations, and apply equation (18). This procedure will result in

$$\overline{C}(a_5) - \overline{C}(b_4) = \epsilon_{21}\left[\nabla_{\overline{V}}\varphi \times \overline{V}(b_4) + \nabla_{\overline{r}}\varphi \times \overline{r}(b_4)\right] \tag{21}$$

Since $\overline{C}$ is constant during each phase

$$\overline{C}(a_5) = \overline{C}(b_5) \tag{22}$$

Using equations (17.19) and (17.20) yields

$$\overline{C}(b_5) = -\hat{h}_o \times \left[\epsilon_{26}\hat{V}(b_5) + \epsilon_{25}\hat{r}(b_5)\right] \tag{23}$$

This equation was derived by using the results of reference 3, where it is shown that $\nabla_{\overline{V}} y \times \overline{V} + \nabla_{\overline{r}} y \times \overline{r} = \overline{0}$ if $y = y(r, V, \overline{r} \cdot \overline{V})$. Since the return time T and the apogee and perigee delta velocities are of this form, the corresponding vector product sums are zero. From equation (23)

$$\overline{C}(b_5) \cdot \hat{h}_o = 0 \tag{24}$$

Taking the scalar product of equation (21) with h_o then gives

$$\epsilon_{21} = \frac{\overline{C}(b_4) \cdot \hat{h}_o}{\left[\nabla_{\overline{V}}\varphi \times \overline{V}(b_4) + \nabla_{\overline{r}}\varphi \times \overline{r}(b_4)\right] \cdot \hat{h}_o} \tag{25}$$

Given ϵ_{21} and $\overline{X}(b_4)$, let

$$\overline{X} = \overline{X}(b_4) + \epsilon_{21}\nabla_{\overline{V}}\varphi \tag{26}$$

With this definition, equation (17.14) becomes

$$\overline{X}(a_5) = \epsilon_{20}\overline{V}(b_4) + \overline{X} \tag{27}$$

To determine the discontinuity in $\overline{X}$ and $\overline{\mu}$, ϵ_{20} must be evaluated. This may be done as follows. From equation (11)

$$\tau(a_5) - \tau(b_4) = -\beta(a_5)K(a_5) \tag{28a}$$

and

$$\tau(a_4) - \tau(b_3) = \beta(b_3)K(b_3) \tag{28b}$$

From equations (28) and (17.18) the following equation is obtained:

$$\beta(a_5)K(a_5) = \beta(b_3)K(b_3) \tag{29}$$

Since $\dot{\sigma} = 0$ on a coast phase (σ = constant), equations (17.13), (17.16), and (17.17) give $\sigma(a_5) = \sigma(b_3)$. Without loss of generality, assume $\beta(a_5) = \beta(b_3) \neq 0$. Then equation (29) reduces to

$$\lambda(a_5) = \frac{m(a_5)}{m(b_3)}\lambda(b_3) \tag{30}$$

Now $\lambda(a_5)$ may be substituted from equation (27) and the resulting equation solved for ϵ_{20}, giving

$$\epsilon_{20} = -\frac{1}{V(b_4)} \times \left\{ \overline{X} \cdot \hat{V}(b_4) \pm \sqrt{\left[\overline{X} \cdot \hat{V}(b_4)\right]^2 + \left[\frac{m(a_5)\lambda(b_3)}{m(b_3)}\right]^2 - X^2} \right\} \tag{31}$$

Choice of + or - sign can be determined as follows. Assume the payload is zero, that is, $m(a_5) = m(b_3)$. Also if the declination is not specified, equation (26) becomes $\overline{X} = \overline{X}(b_4)$. Furthermore, if payload-separation coast phase is zero, $\overline{X}(b_4) = \overline{X}(b_3)$. With these assumptions, equation (31) becomes

$$\epsilon_{20} = -\frac{1}{V(b_4)}\left[\overline{X}(b_4) \cdot \hat{V}(b_4) \pm \overline{X}(b_4) \cdot \hat{V}(b_4)\right]$$

A choice of - sign implies that $\epsilon_{20} = 0$ and that the

thrust direction is continuous at a_5 and is essentially pointed along the velocity vector. However, to bring the Tug back, velocity must be reduced below escape velocity and the thrust direction should be opposite to the velocity vector. Therefore, the + sign should be used in equation (31).

Variational Final Conditions at Retroburn Completion

In this section, variational final conditions will be derived at retorburn completion. Substituting equations (17.19), (17.20), and (17.25) into equation (17.24) gives

$$-\left[\epsilon_{25}\hat{r}(b_5) + \epsilon_{26}\hat{V}(b_5)\right] \cdot \frac{\partial \hat{h}_o}{\partial T_D}$$

$$\times \left[-\frac{G}{r^3(b_5)} \nabla_{\overline{V}} T \cdot \overline{r}(b_5) + \nabla_{\overline{r}} T \cdot \overline{V}(b_5)\right] - \sigma(b_5)\frac{m(b_5)}{V_e}$$

$$\times \left[-\frac{G}{r^3(b_5)} \nabla_{\overline{V}} \Delta V_T \cdot \overline{r}(b_5) + \nabla_{\overline{r}} \Delta V_T \cdot \overline{V}(b_5)\right]$$

$$+ \beta(b_5)\left[\frac{V_e \lambda(b_5)}{m(b_5)} - \sigma(b_5)\right]$$

$$= \left[\epsilon_{25}\hat{r}(b_5) + \epsilon_{26}\hat{V}(b_5)\right] \cdot \frac{\partial \hat{h}_o}{\partial T_D} \qquad (32)$$

However,

$$-\frac{G}{r^3(b_5)} \nabla_{\overline{V}} T \cdot \overline{r}(b_5) + \nabla_{\overline{r}} T \cdot \overline{V}(b_5) = \frac{dT}{dt}$$

and

$$-\frac{G}{r^3(b_5)} \nabla_{\overline{V}} \Delta V_T \cdot \overline{r}(b_5) + \nabla_{\overline{r}} \Delta V_T \cdot \overline{V}(b_5) = \frac{d\,\Delta V_T}{dt}$$

These equations are valid on a coast phase, where the delta velocity required to return the Tug to the SS orbit remains constant; and $d\,\Delta V_T/dt = 0$. Similarly, the change in return time is equal to the change in time along the coast arc but opposite in sign, that is, $dT/dt = -1$. Substituting these results into equation (32) gives

$$\sigma(b_5) = \frac{V_e \lambda(b_5)}{m(b_5)} \qquad (33)$$

The arbitrary constants ϵ_{25} and ϵ_{26} can be evaluated by taking the scalar product of equation (23) with $\overline{r}(b_5)$ and $\overline{V}(b_5)$, giving

$$\epsilon_{26} = -\frac{\overline{\lambda}(b_5) \cdot \hat{h}(b_5)}{\hat{h}(b_5) \cdot \hat{h}_o} V(b_5) \qquad (34)$$

and

$$\epsilon_{25} = -\frac{\overline{\mu}(b_5) \cdot \hat{h}(b_5)}{\hat{h}(b_5) \cdot \hat{h}_o} r(b_5) \qquad (35)$$

Two variational conditions may now be obtained by taking the scalar product of equation (17.19) with $\nabla_{\overline{V}} \Delta V_T$ and equation (17.20) with $\nabla_{\overline{r}} \Delta V_T$ and using equation (33):

$$\left(\overline{\lambda}(b_5) + \lambda(b_5)\nabla_{\overline{V}} \Delta V_T + \frac{\epsilon_{26}}{V(b_5)}\left\{\hat{h}_o - \left[\hat{h}_o \cdot \hat{V}(b_5)\right]\hat{V}(b_5)\right\}\right.$$

$$\left. + \left[\epsilon_{25}\hat{r}(b_5) + \epsilon_{26}\hat{V}(b_5)\right] \cdot \frac{\partial \hat{h}_o}{\partial T_D} \nabla_{\overline{V}} T\right) \cdot \nabla_{\overline{V}} \Delta V_T = 0 \qquad (36)$$

$$\left(\overline{\mu}(b_5) + \lambda(b_5)\nabla_{\overline{r}} \Delta V_T + \frac{\epsilon_{25}}{r(b_5)}\left\{\hat{h}_o - \left[\hat{h}_o - \hat{r}(b_5)\right]\hat{r}(b_5)\right\}\right.$$

$$\left. + \left[\epsilon_{25}\hat{r}(b_5) + \epsilon_{26}\hat{V}(b_5)\right] \cdot \frac{\partial \hat{h}_o}{\partial T_D} \nabla_{\overline{V}} T\right) \cdot \nabla_{\overline{r}} \Delta V_T = 0 \qquad (37)$$

In these equations, $\partial \hat{h}_o/\partial T_D$ is given by the vector

$$\frac{\partial \hat{h}_o}{\partial T_D} = \frac{1}{h_o}\left[\frac{\partial \overline{h}_o}{\partial T_D} - \left(\hat{h}_o \cdot \frac{\partial \overline{h}_o}{\partial T_D}\right)\hat{h}_o\right] \qquad (38)$$

where

$$\frac{\partial \overline{h}_o}{\partial T_D} = \frac{\partial \Omega}{\partial T_D}\left(r_{11}V_{13} - r_{13}V_{11}, r_{12}V_{13} - r_{13}V_{12}, 0\right)$$

The components of $\overline{r}_1$ and $\overline{V}_1$ in this equation are given by

$$\hat{r}_{1j} = \overline{r}_1 \cdot \hat{\ell}_j$$

$$V_{1j} = \overline{V}_1 \cdot \hat{\ell}_j$$

The third variational condition is given by using equations (17.24), (17.25), and (33) as

$$- \frac{G}{r^3(b_5)} \bar{\lambda}(b_5) \cdot \bar{r}(b_5) + \bar{\mu}(b_5) \cdot \bar{V}(b_5)$$

$$- \left[\epsilon_{25}\hat{r}(b_5) + \epsilon_{26}\hat{V}(b_5)\right] \cdot \frac{\partial \hat{h}_o}{\partial T_D} = 0 \qquad (39)$$

Variational Conditions at Completion of First Outbound Burn and Start of Second Outbound Burn

Integrating equation (11) and applying equations (17.6) and (17.10) gives

$$\sigma(b_1) = \frac{V_e \lambda(b_1)}{m(b_1)} \qquad (40a)$$

and

$$\sigma(a_3) = \frac{V_e \lambda(a_3)}{m(a_3)} \qquad (40b)$$

Since σ is constant on a coast phase, equations (17.5) and (17.9) give $\sigma(a_3) = \sigma(b_1)$. Therefore, since $m(b_1) = m(a_3)$, one variational final condition is given by

$$\lambda(a_3) - \lambda(b_1) = 0 \qquad (41)$$

The second variational condition is derived based on the constancy of the Hamiltonian on each phase and equations (17.22) to (17.25). It is given by

$$- \frac{G}{r^3(b_2)} \bar{\lambda}(b_2) \cdot \bar{r}(b_2) + \bar{\mu}(b_2) \cdot \bar{V}(b_2) + \tau(b_2)$$

$$- \left[\epsilon_{25}\hat{r}(b_5) + \epsilon_{26}\hat{V}(b_5)\right] \cdot \frac{\partial \hat{h}_o}{\partial T_D} = 0 \qquad (42)$$

where

$$\tau(b_2) = \int_{a_3}^{b_3} K \frac{\partial \beta}{\partial \xi} \, d\xi + \int_{a_5}^{b_5} K \frac{\partial \beta}{\partial \xi} \, d\xi \qquad (43)$$

If the Tug has a constant flow rate, $\tau(b_2)$ is equal to zero and $\dot{\tau}$ need not be numerically integrated.

Initial and Final Conditions

The initial adjoint variables are unknown and must be guessed at in solving the two-point boundary value problem. As was shown in reference 4, multipliers $\bar{\lambda}$ and $\bar{\mu}$ can be computed from physically more meaningful parameters, such as the vehicle pitch attitude ψ, pitch rate $\dot{\psi}$, yaw attitude δ, yaw rate $\dot{\delta}$, and $\lambda(a_1)$ and $\dot{\lambda}(a_1)$. With these changes in variables the initial and associated final conditions are given by

Initial condition	Final conditions	
$\psi(a_1)$	$\hat{r}(b_5) \cdot \hat{h}_o = 0$	(44.1)
$\dot{\psi}(a_1)$	$\hat{V}(b_5) \cdot \hat{h}_o = 0$	(44.2)
$\delta(a_1)$	$\varphi\left[r(b_4), V(b_4)\right] - \varphi_D = 0$	(44.3)
$\dot{\delta}(a_1)$	Equation (36)	(44.4)
$u(a_1)$	Equation (37)	(44.5)
$m(a_5) - m(b_4)$	$m(b_5) - m_{li} e^{\Delta V_T / V_e} = 0$	(44.6)
T_D	Equation (39)	(44.7)
b_1	Equation (41)	(44.8)
b_2	Equation (42)	(44.9)
$\lambda(a_1)$	$\sigma(a_5) = \sigma(b_4) = 1$	(44.10)
$\dot{\lambda}(a_1)$	$\bar{C}(a_1) \cdot \hat{h}(a_1) = 0$	(44.11)
b_3	$E\left[r(b_4), V(b_4)\right] - E_D = 0$	(44.12)
b_5	$b_5 - a_1 + T - T_D = 0$	(44.13)

Final condition (44.10) can be satisfied by scaling the problem by $\lambda(a_1)$. Therefore, it is omitted from the numerical iteration. Final condition (44.11) is used to compute $\dot{\lambda}(a_1)$, as shown in reference 4. Final conditions (44.12) and (44.13) are used as cutoff conditions to determine b_3 and b_5. With these simplifications the number of final conditions to be satisfied for the perigee propulsion case is reduced to nine, namely, conditions (44.1) to (44.9). For the case without perigee propulsion, conditions (44.8) and (44.9) do not apply, and the number of final conditions to be satisfied is reduced to seven.

The two-point boundary value problem is solved by using a Newton-Raphson numerical iteration technique. The iteration is terminated when the percent of predicted payload change and the absolute value of the normalized final conditions are less than 10^{-5}.

Results and Discussion

The method and equations derived in the previous sections were applied to a typical cryogenic Tug configuration and a set of planetary injection conditions. The results of this analysis are presented in this section.

Propulsion and weight characteristics for the reusable Tug are given in table I. The initial weight of the

Tug and payload is assumed to be fixed to remain within SS payload capability. To satisfy this constraint, Tug propellant load must be varied with payload weight to maintain this initial weight. Engine thrust corresponds to the RL-10 engine currently in use on the Centaur cryogenic upper stage, but engine specific impulse represents a state-of-the-art uprated version of the same engine. To account for losses and flight performance reserves, engine specific impulse is reduced by 2 percent.

The sample case selected (table II) is a typical inner planet (Mars, Venus) mission, with a mission energy of 12 $(km/sec)^2$, an initial SS circular-orbit altitude of 185 km, and a SS orbital inclination of 28.5°. This SS orbital inclination was chosen based on the results of reference 1, where it is shown that maximum Tug performance is obtained (for declinations less than 30°) when departing from this SS orbital inclination. Payload-separation coast time (the time from outbound burn cutoff to the start of retroburn) is assumed to be 10 minutes.

To show the payload gain due to perigee propulsion, Tug payload capability without perigee propulsion for optimum trip times is also presented.

Figures 1 to 7 present results without perigee propulsion; figures 8 to 16 contain results for perigee propulsion cases. The data are given as a function of the declination of the outgoing asymptote (DLA), which was parametrically varied.

It is also shown in reference 1 that there are two solutions for each declination and that the payload curves are symmetric about a 0° declination. Therefore, the data presented herein are restricted to positive declinations. Right ascension of the outgoing asymptote was not specified in the analysis, and consequently an "optimal pseudo right ascension" is generated for each DLA. Pseudo right ascension is defined as the longitude of the projection of the outgoing asymptote in the equatorial plane measured from the initial SS orbital ascending node. Right ascension may be computed by adding the pseudo right ascension to the longitude of the SS orbital ascending node measured from the vernal equinox. Since the longitude of the SS orbital ascending node is determined by SS launch time, any desired right ascension may be obtained by selecting the proper launch time.

Optimal pseudo right ascension is presented in figure 1 for the case without perigee propulsion. To distinguish between the two solutions on all figures, a solid and a dashed line are used. The solution given by the dashed line will be referred to as solution 1, and the one given by the solid line as solution 2. In the region of single solutions, where DLA exceeds SS orbital inclination, a solid line is used. Note that for 0° DLA, the outgoing asymptotes associated with the two solutions point in opposite directions. As DLA is increased the outgoing asymptotes move closed together until the two solutions degenerate into a single solution. At this point the outgoing asymptote has a pseudo right ascension of approximately 90°. For DLA's beyond the SS orbital inclination, the pseudo right ascension remains nearly constant

The Tug departure point from the initial SS orbit was determined during the optimization, and the results are presented in figure 2. Departure arguments of latitude of the two solutions are also 180° apart for 0° DLA and converge to about 260° as the DLA approaches the SS orbital inclination.

Optimum total trip time (the time from Tug departure from the initial SS orbit to return to the rendezvous orbit) is given in figure 3. Total trip times for the two solutions are nearly the same and decrease from approximately 26 to 21.5 hr as DLA is increased from 0° to 30°. Total trip time varies inversely with the duration of the retroburn. The shorter the retroburn, the more elliptic the return orbit, and consequently the total trip time increases. Velocity loss during retroburn is proportional to the burn time. Therefore, as total trip time is increased, the velocity loss during retroburn decreases. However, the nodal correction due to SS orbital precession will increase with total trip time, which increases the velocity loss to correct for nodal precession. Therefore, there is a balance between these two effects that determines the optimal trip time. Variation in trip time is due to changes in orbital geometry and associated nodal correction during outbound and retroburns. The sharp increase in total trip time for DLA's larger than the SS orbital inclination can be explained when changes in orbital inclination during outbound burn are considered. It is well known from orbital geometry that orbital inclination at injection must be at least as large as the magnitude of the desired DLA. Therefore, large inclination changes are made during both outbound burn and retroburn for DLA's larger than the SS orbital inclination. Departure arguments of latitude for these cases are approximately 260°, and the outbound burn covers about a 90° arc. Therefore, the complete burn occurs before nodal passage. Since orbital inclination must be increased, as was mentioned earlier and the line of nodes tends to move retrograde during the inclination change, it becomes easy to make large nodal changes during the outbound burn. These nodal changes are in the same direction as the SS nodal precession, so longer trip times become optimum.

Nodal correction during the outbound burn and total nodal correction (during outbound burn and retroburn) are given in figure 4. Total nodal corrections for the

two solutions are very close and differ only because of the slightly different trip times for the two solutions. However, the outbound nodal correction for one solution is large and for the other it is small. This is explained by the location of the outbound burn. For the case with large nodal correction during outbound burn, the outbound burn starts near or after nodal passage (fig. 2). Since the outbound burn arc is approximately 90°, the Tug burn continues through maximum latitude, which is an optimal region in which to change the line of nodes. For the case with small nodal correction during outbound burn, the burn generally takes place near the ascending nodal passage, where it is difficult to change the node. Also note that for large DLA's the total nodal correction increases faster than the nodal change during the outbound burn; that is, larger nodal changes are made during the retroburn. This is expected, since large inclination changes are being made during this burn to return the Tug to the SS, and it becomes optimum to combine nodal correction with the inclination change.

Figure 5 presents the inclination of the hyperbolic orbit containing the outgoing asymptote. There is a maximum inclination change during outbound burn of ±1.5 deg for DLA's less than the SS orbital inclination. For the first solution (dashed line) the outbound burn starts ahead of the ascending line of nodes (fig. 2) and ends past it. In this region it is difficult to change the line of nodes, and nodal change (fig. 4) is small. To move the node retrograde for these solutions, the orbital inclination must be increased, as shown in figure 5. For the second solution (solid line) the outbound burn starts past nodal passage (fig. 2) and continues through maximum latitude, which is an optimal region in which to change the node. Most of the nodal change is done during this burn (fig. 4). Since the burn is past the node, orbital inclination must be decreased to move the node retrograde (fig. 5). As the DLA approaches the SS orbital inclination, the inclination at injection must be increased to meet the DLA requirements, and for the single solutions the orbital inclination is increased to coincide with the DLA.

Tug payload capability without perigee propulsion for the two solutions is given in figure 6. The two solutions have nearly the same performance (maximum difference, 20 kg out of 4750 kg). Payload capability decreases with increasing DLA. This decrease is approximately 90 kg between 0° and 30° DLA. For DLA's higher than 30° the payload decreases rapidly because of the large inclination changes required, as discussed earlier.

Velocity losses encountered during outbound and inbound trajectory portions are presented in figure 7. Velocity loss is defined as the difference between the velocity supplied by the Tug (based on the amount of propellant used and the ideal rocket equation) and the ideal mission impulsive velocity. Ideal mission impulsive velocity is defined as the velocity needed above circular-orbit velocity at a 185-km altitude in order to reach a given energy. Total velocity loss gradually increases with increasing DLA for DLA's less than 30°. As DLA is increased beyond 30°, the velocity losses increase very rapidly, again because of the large inclination changes being made. Note that the solutions given by the dashed line have larger total velocity losses than the solutions given by the solid line, yet the payload for these solutions is higher (fig. 6). This apparent incongruity is due to the unequal effect of velocity loss on payload during outbound and inbound trajectory portions. The effect of the outbound velocity loss on payload is almost twice the effect of the inbound velocity loss. Therefore, for the solutions given by the dashed line the payload increase due to lower outbound velocity losses is greater than the payload decrease due to higher inbound velocity losses when compared with the solutions given by the solid line.

The outbound velocity losses of figure 7 indicate that large velocity losses are associated with the finite thrust level of the reusable Tug. These losses can be reduced substantially by using the technique called "perigee propulsion." With perigee propulsion the outbound burn is split into two separate burns. The first outbound burn puts the Tug and payload into an elliptic orbit. The Tug is allowed to coast almost to the perigee of this orbit, where a second outbound burn takes place. The second outbound burn continues until the target conditions are satisfied. After payload injection at the specified conditions, the flight sequence is the same as that without perigee propulsion. The lengths of the first outbound burn and the coast phase following it are optimized; that is, they are selected to maximize payload.

In figures 8 and 9, the pseudo right ascension and the departure argument of latitude are given, respectively, as a function of DLA for the case with perigee propulsion. These figures are very similar to those discussed for the case without perigee propulsion and will not be elaborated on further.

Optimum total trip time is presented in figure 10. For these cases the first solution has a shorter trip time (dashed line) than the second solution. The first solutions also have shorter first outbound burns, as shown in figure 11. The first outbound burn varies with varying DLA from about 630 sec to 740 sec, as compared with the total outbound burn of approximately 1100 sec for the non-perigee-propulsion case. The period of the elliptic orbit achieved at first outbound burn completion varies between 4 and 6 hr. The second outbound burn is initiated along this orbit at the optimum true anomalies given in figure 12.

The total outbound nodal correction and the inclination of the hyperbolic orbit containing the outgoing asymptote are presented in figures 13 and 14, respectively, and are similar to those without perigee propulsion. The larger difference in total required nodal correction between the two solutions with perigee propulsion than between the two solutions without perigee propulsion is caused by a larger difference in total trip time.

Payload capability with perigee propulsion is given in figure 15. The maximum payload difference between the two solutions is about 100 kg out of about 5200 kg. Payload again drops off rapidly as DLA is increased beyond 30^0. Velocity losses with perigee propulsion are substantially lower than without perigee propulsion, as seen by comparing figure 16 with figure 7. This results in the improved performance using perigee propulsion seen in figure 15.

For comparison, the ideal impulsive payload capability without nodal correction and the payload capability including nodal correction with and without perigee propulsion are given in figure 17. Ideal payload capability for the baseline Tug analyzed is 5760 kg, as compared with a maximum payload capability with perigee propulsion of 5100 kg and without perigee propulsion of 4700 kg. This shows that by using perigee propulsion the payload loss due to gravitational and other trajectory shaping effects can be reduced by about 40 percent. Of course, doing so requires an additional burn with its associated startup and shutdown losses, as well as additional guidance requirements that must be considered in evaluating the advantages of perigee propulsion.

Summary and Conclusions

Equations are derived in this paper that can be used to maximize the payload capability of a reusable Tug at energies beyond Earth escape with and without the use of perigee propulsion. The analysis includes correction for SS orbit nodal precession, while the total trip time (time from Tug departure to return to the SS orbit) is optimized.

Based on the results presented for the baseline Tug and baseline mission, the following conclusions can be made:

1. For trajectories not using perigee propulsion the payload losses due to gravitational and other trajectory shaping constraints are large (970 kg out of an ideal payload capability of 5760 kg).

2. The payload loss can be reduced by approximately 40 percent by using perigee propulsion. (Payload loss with perigee propulsion is 570 kg.)

3. Optimal total trip time varies from about 21 to 26 hr without perigee propulsion and from 18 to 24 hr with perigee propulsion for a declination range of 0^0 to 30^0.

4. Any declination between -30^0 and $+30^0$ may be reached by departing from a 28.5^0 inclined SS orbit. The variation in payload for this declination range is small compared with the nominal payload capability. For higher declinations the SS orbital inclination must be increased to avoid large payload degradation.

5. Optimal round-trip reusable Tug trajectories including the SS orbit nodal precession to energies beyond Earth escape with and without perigee propulsion can be obtained by a straightforward Newton-Raphson iteration technique using the methodology developed herein.

Appendix - Symbols

a	time at beginning of a phase, sec
b	time at end of a phase, sec
C	defined by eq. (18), kg-sec
DLA	declination of outgoing asymptote, deg
E	energy, m^2/sec^2
e	eccentricity
$\hat{f}$	thrust direction defined by eq. (13)
G	gravitational constant of Earth, m^3/sec^2
H	Hamiltonian, kg
H*	augmented Hamiltonian, kg
h	angular momentum, m^2/sec
i	inclination, rad
J	oblateness parameter (1.624×10^{-3})
K	kappa function defined by eq. (12), sec
$\hat{\ell}_1, \hat{\ell}_2, \hat{\ell}_3$	right-handed Cartesian coordinate system (vector $\hat{\ell}_1$ points to the initial SS orbital line of nodes and $\hat{\ell}_3$ points to the North Pole)
m	mass, kg
P	orbital period, sec
p	semilatus rectum, m
q_l	constraints
R_E	radius of Earth (6.37816×10^6 m)
r	radius, m
T	return time, sec
T_D	total trip time, sec
t	time, sec
Δt	payload-separation coast time, sec

u	argument of latitude, rad
V	velocity, m/sec
ΔV_a	apogee delta velocity, m/sec
ΔV_p	perigee delta velocity, m/sec
ΔV_T	total delta velocity ($\Delta V_T = \Delta V_a + \Delta V_p$), m/sec
X	defined by eq. (26), kg-sec^2/m
y	dummy variable
β	mass flow rate, kg/sec
γ	multiplier associated with thrust direction, kg
δ	yaw attitude, rad
ϵ	multiplier associated with trajectory constraints
ξ	dummy variable, sec
λ	adjoint multiplier associated with velocity, kg-sec^2/m
μ	adjoint multiplier associated with position, kg-sec/m
σ	adjoint multiplier associated with mass, sec
τ	adjoint multiplier associated with ξ, kg
φ	declination of outgoing asymptote, rad
ψ	pitch attitude, rad
Ω	longitude of line of nodes, rad

Subscripts:

a	apogee
e	exhaust
H	hardware
l	variable index
o	precessed SS orbit at time T_D
p	perigee

Superscripts:

'	time derivative
⁻	vector
^	unit vector

References

1. Borsody, J., "Optimal Three Dimensional Reusable Tug Trajectories for Planetary Missions Including Correction for Nodal Precession," TN D-8168, 1976, NASA.

2. Wolverton, R. W., Flight Performance Handbook for Orbital Operations, John Wiley & Sons, Inc., New York, 1963.

3. Spurlock, O. F. and Teren, F., "Optimum Launch Trajectories for the ATS-F Mission," AIAA Paper 70-1051, Santa Barbara, Calif., 1970.

4. Teren, F. and Spurlock, O. F., "Optimum Three-Dimensional Launch Vehicle Trajectories with Attitude and Attitude Rate Constraints," TN D-5117, 1969, NASA.

Table I. - Baseline Tug characteristics

Tug initial weight (including payload), kg	28 922
Tug burnout weight, kg	2767
Engine thrust, N	66 723
Engine specific impulse, sec	460
Performance reserve, percent of specific impulse	2

Table II. - Baseline mission characteristics

Mission energy, (km/sec)^2	12
Range of declination, deg	0 to 34
Payload-separation coast time, min	10
Initial SS orbital altitude, km	185
Initial SS orbital inclination, deg	28.5

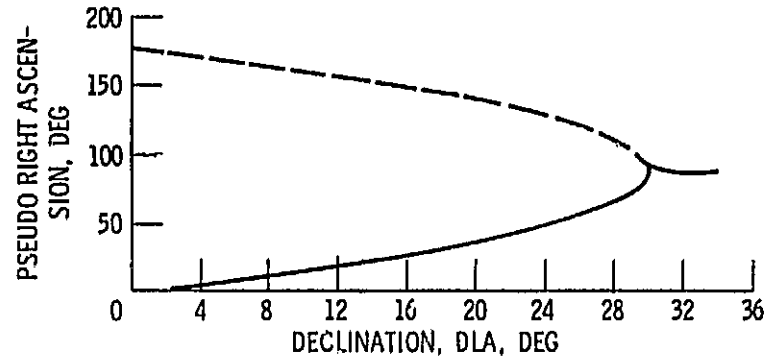

Figure 1. - Pseudo right ascension of outgoing asymptote measured counterclockwise in equatorial plane from initial Space Shuttle orbit ascending node - without perigee propulsion.

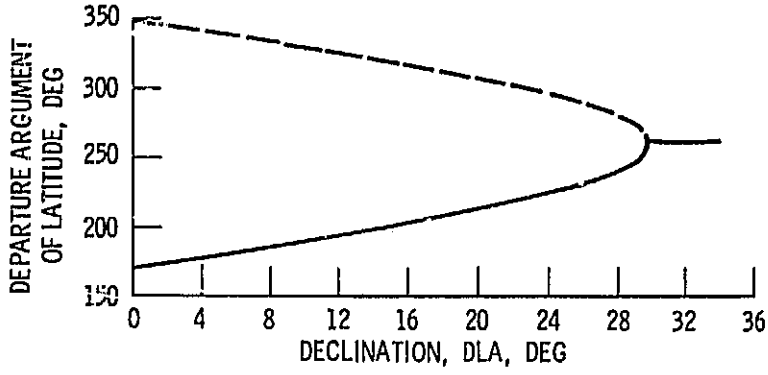

Figure 2. - Argument of latitude measured in initial Space Shuttle orbit - without perigee propulsion.

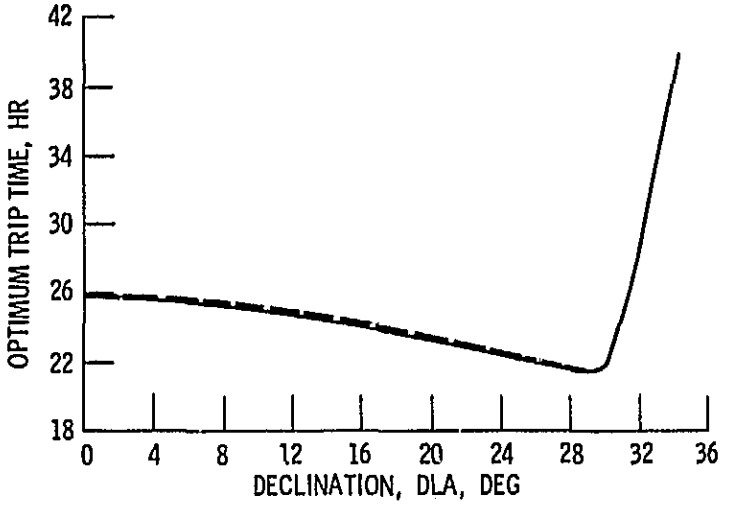

Figure 3. - Optimum Tug trip time from departure from initial Space Shuttle orbit to return to Space Shuttle - without perigee propulsion.

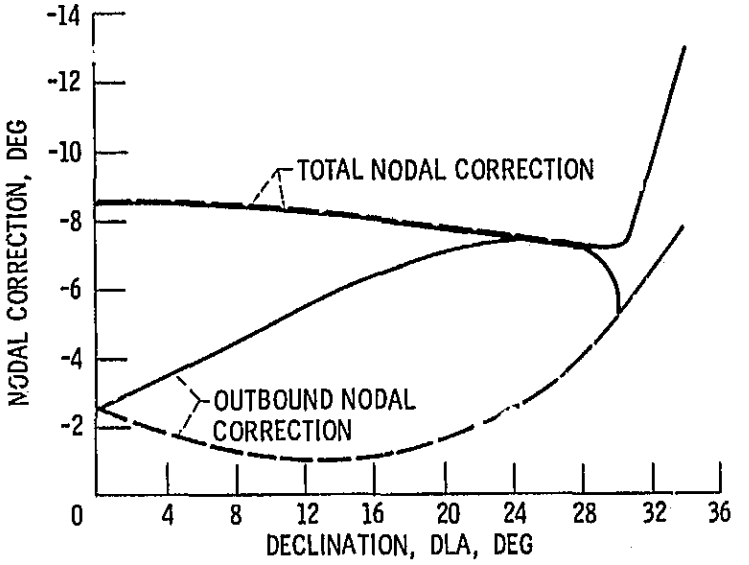

Figure 4. - Nodal shift made during outbound burn and total nodal correction - without perigee propulsion.

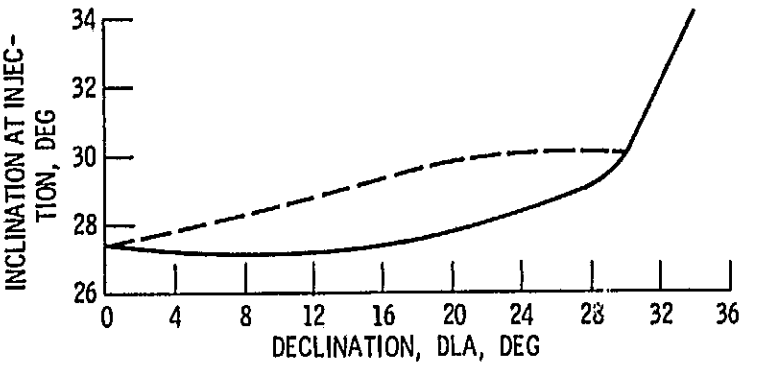

Figure 5. - Inclination of hyperbolic orbit containing desired outgoing asymptote - without perigee propulsion.

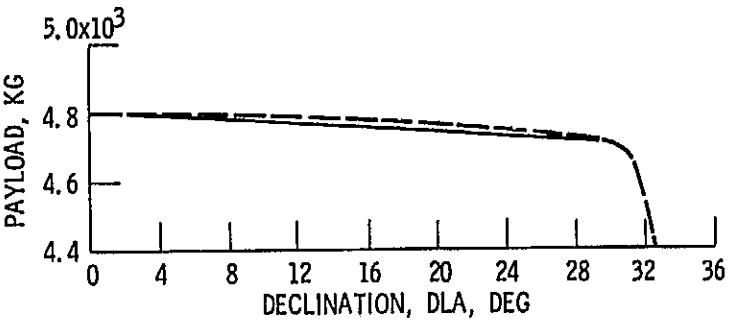

Figure 6. - Tug payload capability - without perigee propulsion.

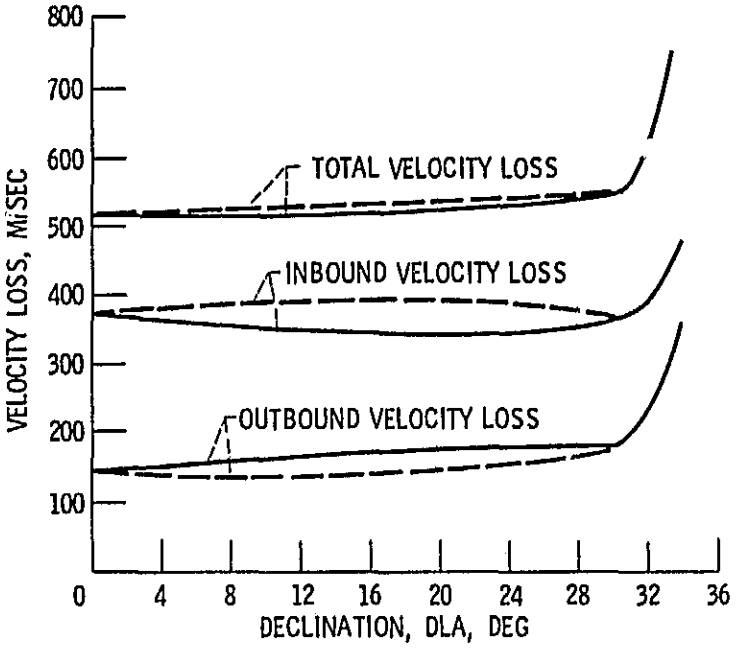

Figure 7. - Velocity loss on outbound and inbound trajectory legs - without perigee propulsion.

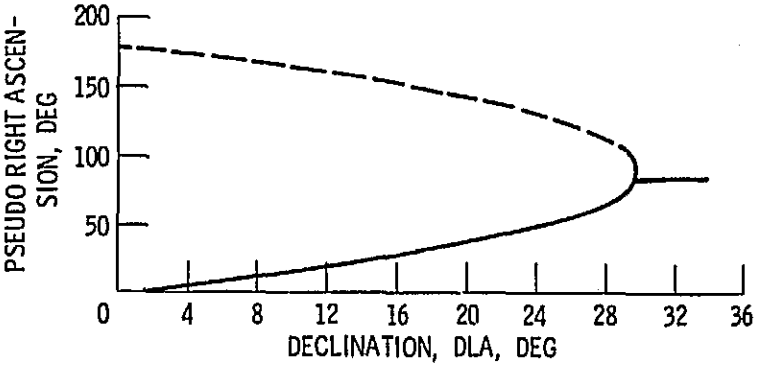

Figure 8. - Pseudo right ascension of outgoing asymptote measured counterclockwise in equatorial plane from initial Space Shuttle orbit ascending node - with perigee propulsion.

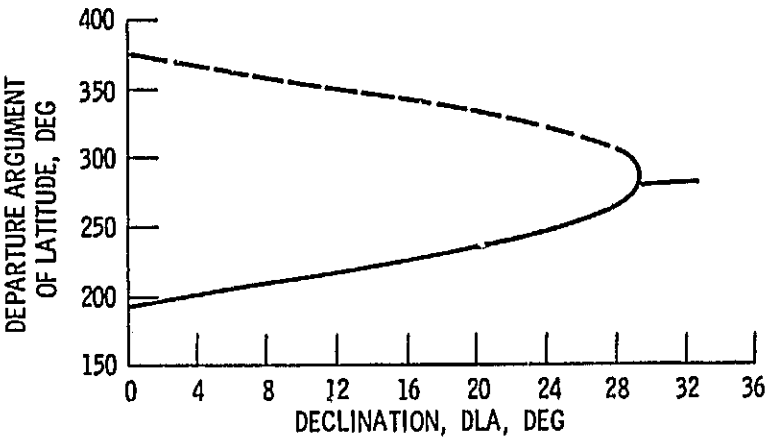

Figure 9. - Argument of latitude measured in initial Space Shuttle orbit - with perigee propulsion.

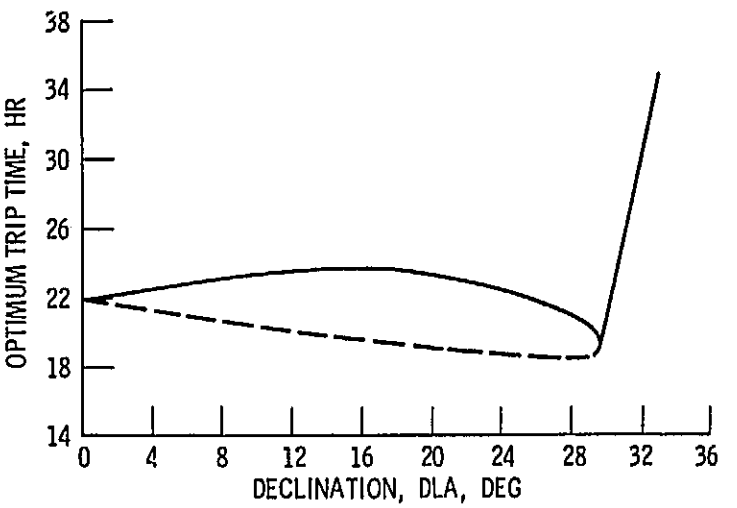

Figure 10. - Optimum Tug trip time from departure from initial Space Shuttle orbit to return to Space Shuttle - with perigee propulsion.

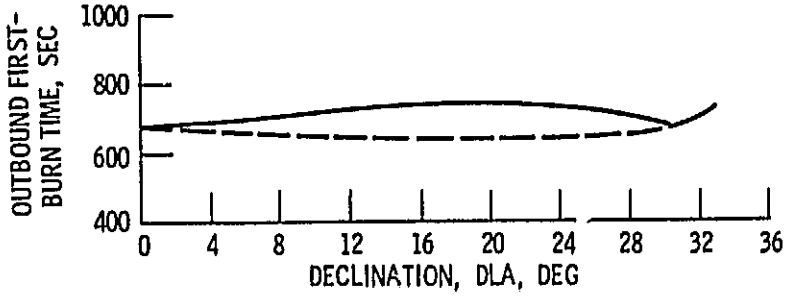

Figure 11. - Tug outbound first-burn time - with perigee propulsion.

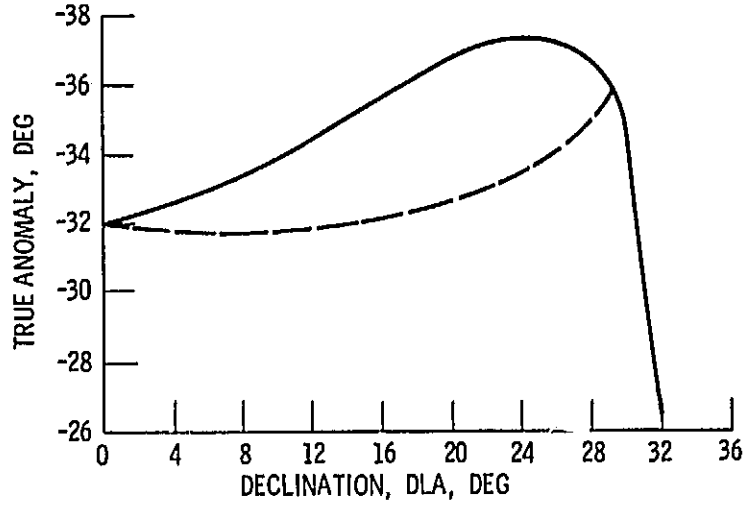

Figure 12. - True anomaly at start of second outbound burn - with perigee propulsion.

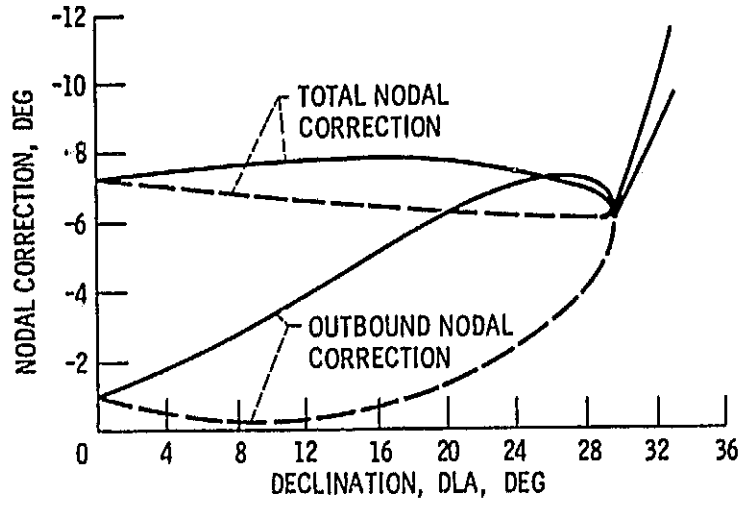

Figure 13. - Nodal shift made during outbound burns and required total nodal correction - with perigee propulsion.

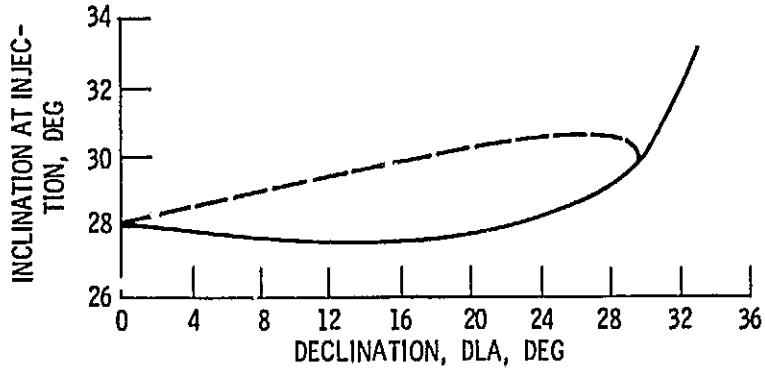

Figure 14. - Inclination of hyperbolic orbit containing desired outgoing asymptote - with perigee propulsion.

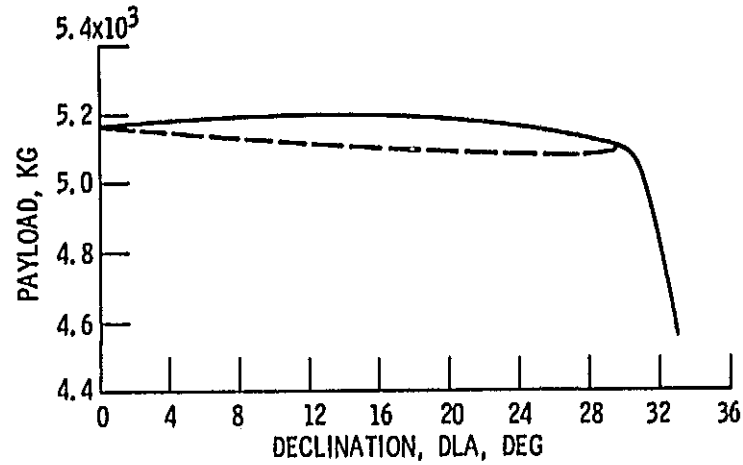

Figure 15. - Tug payload capability - with perigee propulsion.

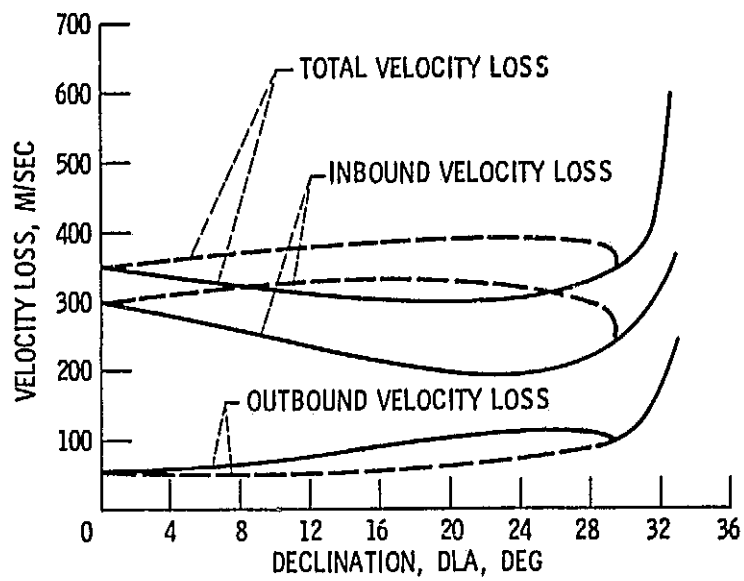

Figure 16. - Velocity loss on outbound and inbound trajectory legs - with perigee propulsion.

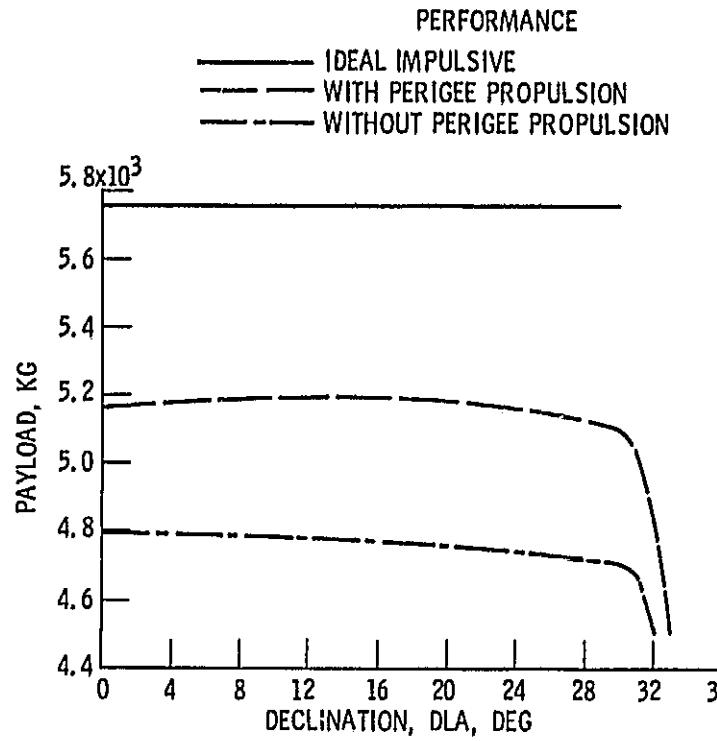

Figure 17. - Comparison of maximum Tug payload capability, with and without perigee propulsion, with ideal performance.